Contrib. Mineral. Petrol. 72, 367–386 (1980)

Contributions to Mineralogy and Petrology

Geology, Petrography, and Petrology of Pinzon Island, Galapagos Archipelago

Hartmut W. Baitis [1] and Marilyn M. Lindstrom [2]

[1] Noranda Exploration, Inc., 2436 West Central, Missoula, Montana 59801, USA
[2] Department of Earth and Planetary Sciences, Washington University, St. Louis, Missouri 63130, USA

Abstract. Three stratigraphic units based on geologic relationships and paleomagnetic observations may be distinguished on Pinzon Island. The oldest unit is a broad shield which forms the main body of the island and was erupted during a period of reversed magnetic polarity from an area now occupied by a caldera. Subsequent activity was centered about 1.5 km to the north-northwest from vents later engulfed by the collapse of a younger caldera. The lower portion of this sequence was erupted during a period of transitional pole positions and is overlain by flows of normal polarity. Pinzon has the most diverse suite of differentiated tholeiitic rocks found in the Galapagos Archipelago. Products of eruptive cycles are preserved as sequences of tuffs and flows that have decreasing degrees of differentiation and increasing phenocryst abundance upsection. The sequences may be a consequence of tapping successively deeper levels of compositionally zoned magma chambers. Such a model is consistent with computer calculations utilizing major and trace element data for Pinzon rocks, which suggest that lavas of the island may be related by shallow-level crystal fractionation of observed phenocryst minerals.

Introduction

The Galapagos Islands are on the equator approximately 1,000 km west of the Ecuadorian mainland near the Galapagos Rift, an active spreading center, and at the junction of the ascismic Cocos and Carnegie Ridges. The islands of the Archipelago rise above sea level as small protrusions on an otherwise submerged elongate submarine platform. Pinzon's area of 19 km^2 ranks 12th among the islands which comprise the Archipelago (Fig. 1).

Previous geologic investigations of Pinzon have been very limited. Chubb (1933) mistakenly called Pinzon a 'tuff volcano' devoid of lava fields and apparently did not land on it. McBirney and Williams (1969) present petrographic descriptions and chemical analyses of four samples collected as a part of a regional reconnaissance of the Archipelago. Mapping and sampling of rocks on Pinzon were carried out during several weeks in 1971 and 1973, and a brief summary of its geology has been published as a result of this work (Swanson et al. 1974).

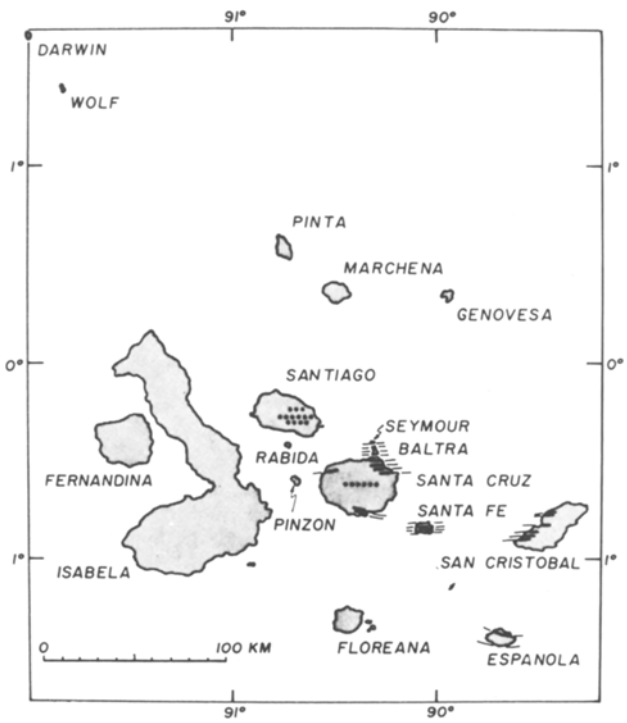

Fig. 1. The Galapagos Archipelago showing location of Pinzon and other major islands. *East-trending solid* and *dotted lines* schematically represent areas of normal fault traces and aligned vents, respectively

0010-7999/80/0072/0367/$04.00

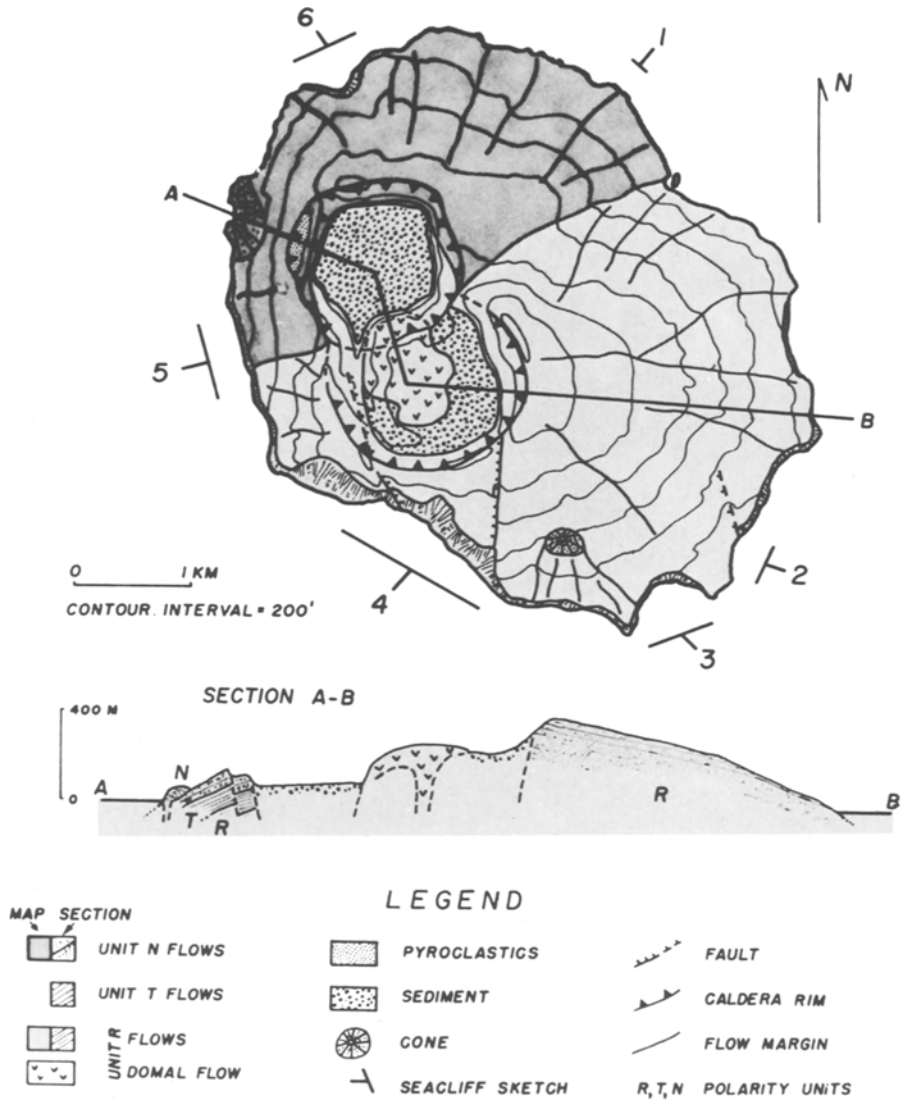

Fig. 2. Geologic map of Pinzon Island. Topographic base from U.S. Hydrographic Chart no. 5936. *Numbers* around island refer to sketches of sea-cliff sections shown in Fig. 3

This paper presents a detailed discussion of the geology of Pinzon, and results of petrographic and geochemical studies of rocks from the island.

Physiography

Marine erosion has reduced the size of Pinzon to 6.5 by 4.5 km (Fig. 2), although, like the smaller Rabida Island 17 km to the north, it is the summit of a much larger volcano. Almost the entire island is girt by high cliffs that allow access in only a few places to the foreshore which, nevertheless, can be traversed along the base of talus slopes for most of the coastline. Sea cliffs more than 50 m in height are developed almost continuously around the southern and western margins of the island and rise over 200 m above the southwestern perimeter of the island.

Above the steep sea cliffs, the rubble- and shrub-covered constructional flanks of Pinzon dip seaward at 8° to 25° from the rims of two overlapping calderas (Fig. 2). The southern caldera has a ragged rim nearly 2 km in diameter, which is cut by several scarps of high-angle normal faults. These flows and the high-angle faults that cut them are only slightly modified by mass wasting, forming terrain covered by large blocks and boulders with very little soil development. The summit of Pinzon, 457 m above sea level, is a ridge along the eastern margin of the southern caldera.

The caldera immediately to the northwest is a younger feature with sharply-defined boundary faults and a broad, flat floor that dips gently northward. This caldera is roughly a kilometer across and 100 to 150 m deep. Its floor is sparsely vegetated and is largely covered with sediment contributed during infrequent storms. Coarser debris is found in an alluvial fan that spreads onto the floor from a canyon that enters the caldera from the southwest.

Pinzon has several deeply eroded cones of cinders and spatter; one is located at the southern tip of the island, and two more are on the northwestern side (Fig. 2).

The young, constructional slopes of the two coalescing shields of Pinzon afford few exposures. However, steeper portions of the caldera walls and the sea cliffs offer excellent exposures of the eruption products that built the subaerial portion of the island.

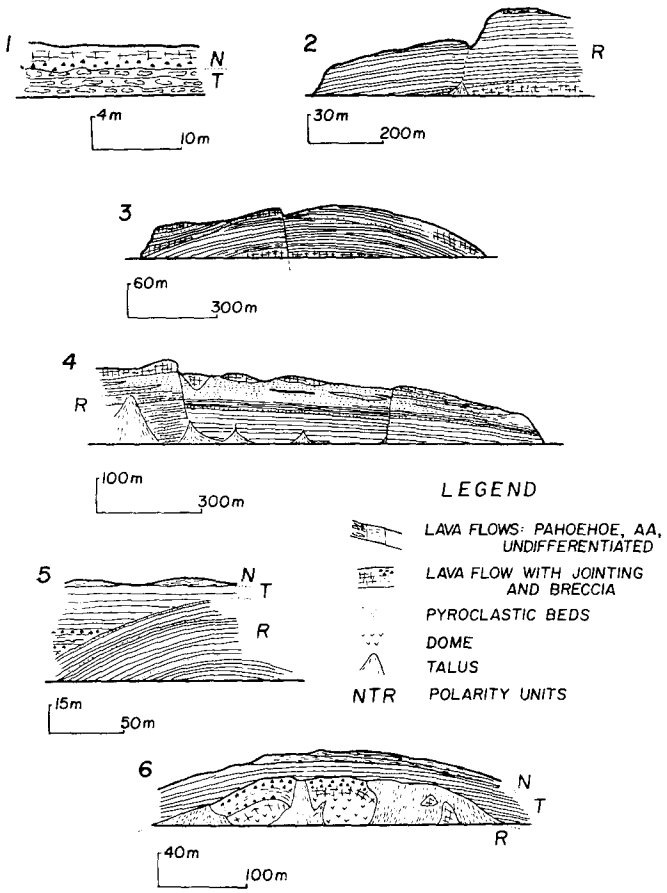

Fig. 3. Pinzon sea-cliff sections noted in Fig. 2

Geology

The geology of Pinzon Island is shown in Figs. 2 and 3. The Pinzon volcanic series can be divided into four units on the basis of paleomagnetic observations and stratigraphic relationships. The oldest unit, denoted R in Figs. 2 and 3, forms the main body of the volcano and was erupted during the Matuyama Reversed Polarity Epoch from the area now occupied by the southern caldera (Swanson et al. 1974). Subsequent activity was centered about 1.5 km to the north-northwest from a vent or localized, interconnected vents later engulfed by the collapse of the younger caldera. The lower portion of this younger sequence was erupted during a period of transitional or intermediate pole positions and is overlain by flows of normal polarity which were probably erupted during the Jaramillo Event of normal polarity. These units are labeled T and N in Figs. 2, 3, and 7. The construction of two coalescing cinder and agglutinate cones (Unit N2) along the northwestern coast of Pinzon represents the end of volcanic activity on the island (Fig. 2). The overall range in ages of rocks exposed on Pinzon is about 1.0 ± 0.2 m.y., although it is possible that Unit N2 may have been erupted during Brunhes time (Swanson et al. 1974).

Volcanic Features

Pahoehoe Flows. Pahoehoe flows are volumetrically the most abundant type of lava involved in the construction of Pinzon. All fifteen analyzed samples of pahoehoe flows were found to be tholeiites or olivine tholeiites.

Numerous pahoehoe sequences several tens of meters thick are well-exposed in the vertical cliff sections of Pinzon and consist of many layers of superimposed pahoehoe toes with no apparent hiatus between different layers. The lack of erosional surfaces and paleosoils within the pahoehoe sequences indicates that large volumes of lavas were erupted in rapid succession.

Pahoehoe toes are often from a few tens of centimeters to more than a meter across, and individual toes may have flowed only a few meters before they became immobile. The flows often exhibit well-developed ropey surfaces with reddish oxidized chilled margins. Vesicles occur throughout many of the flows, and individual toes often increase in vesiularity toward their centers (Fig. 4). Although pahoehoe toes may be formed in submarine environments (Moore 1971), the lack of any other evidence for submarine eruption of the flows or the interbedded tephra sequences indicates a subaerial environment of deposition.

The pahoehoe lavas commonly contain from a few percent to more than 60% phenocrysts. Many porphyritic flows exposed along the southern and western coasts of Pinzon contain concentrically-oriented feldspar phenocrysts, the orientation apparently being due to differential rates of flow through a roughly cylindrical tube (Fig. 5). In addition, consolidation of successive layers of lavas on the walls of a tube has often resulted in a concentric arrangement of vesicles.

Flow differentiation (Simkin 1967; Komar 1972) has occurred in many of the pahoehoe flows (Fig. 6). Differential shear and flowage rates within individual flows commonly has resulted in flows that have extremely porphyritic centers (as much as 60% plagioclase phenocrysts) which may grade downward into phenocryst-free margins. The boundary between crystal-rich and crystal-poor portions of flows is often very sharp and creates problems in selecting representative samples.

Aa and Block Lava Flows. Aa flows are common in Unit R, where they tend to lie below tephra beds and above pahoehoe flows. Near the top of the western sea-cliff section there is a 50-meter-thick block lava flow. The upper part of Unit N is also characterized by aa lavas and thicker blocky flows.

The aa flows are characteristically less than 3 m thick and have well-developed top and bottom flow breccias. Commonly, the flows are relatively aphanitic and have a dark, glassy appearance in hand specimen. Analyses indicate that the aa lavas tend to be more siliceous (average silica contents for analyzed flows of tholeiitic basalt and ferrobasalt composition are: 13 aa lavas – 49.13%; 15 pahoehoe lavas – 48.24%) and were probably more viscous than the pahoehoe flows.

Block lava flows range from a few to more than 50 m in thickness and tend to be restricted to the latest phases of eruptive activity of both Units R and N. Many of these flows are icelandites and are lighter in color than the more mafic lavas. Most flows have irregular breccia zones and a dense inner portion with crudely-developed blocky jointing.

Tephra. The tephra beds of Pinzon vary widely in physical and chemical composition.

Fine-grained tuff beds are exposed in the sea cliffs of the western and southwestern portions of the island. These beds average 50 cm thick (range 5–120 cm) and generally consist of fragments less than a few millimeters in diameter, but often these beds are interlayered with coarser pumice and agglomerate beds. The tuff beds are relatively continuous and show little lateral variation where they are accessible for comparison. The layers are light in color, and juvenile components are often of oceanic dacite or icelandite composition.

Lapilli tuffs are more abundant and average 2.5 m in thickness (range 0.5–20 m), often grading into tuffs that locally contain as

Fig. 4. Typical sequence of pahoehoe toes exposed in southwestern sea cliffs of Pinzon. Individual toes often exhibit an increase in vesicularity toward their centers

Fig. 5. Concentrically-oriented plagioclase crystals in a pahoehoe toe, southern sea cliffs of Pinzon

Fig. 6. Flow differentiation in a thin pahoehoe flow. The flow center is characterized by increased vesicularity and more than 60% plagioclase phenocrysts. Note ropey flowtop surface of underlying flow in *left hand bottom portion of photo*

much as 30% rock fragments. The lithic fragments vary from less than a centimeter to more than one meter in diameter and include coarse-grained gabbro, as well as earlier tuffs and lavas. Commonly the tephra units include pumic-rich layers interbedded with more block-rich layers, along with interbedded thin aphanitic flows.

Only in three parasitic vents shown in Fig. 2 does one find juvenile basaltic tephra. These layers of cinders and spatter are red in color, owing to their higher iron content and advanced state of oxidation. Most of the other tephra beds are restricted to Unit R, but there is one exception in Unit N that is discussed in a later section. The beds in Unit R occur almost exclusively from the southern tip of the island along the western cliffs to the northwestern tip of the island. The restriction of the tuffs to this side of the island may be due in part to the lack of exposure over the other parts of the island and to the proximity of the western cliffs to the major eruptive vent. It is likely, however, that the distribution of the tuffs may be in part related to the effect of prevailing southeasterly winds, and it is not surprising that the tuffs are largely restricted to the western half of Pinzon.

Domes. Two domes, both with reversed polarities but with quite different compositions, were recognized.

A dome and associated flow of icelandite occupy about 0.4 km^2 of the central part of the southern caldera (Fig. 2). The dome is at least 30 m thick at its thickest portion and probably consists of several flows. The blocky lavas locally are flow-banded, commonly altered, and exhibit silicification with vesicle fillings of chalcedony and zeolites. The flows represent the last phases of activity on the main, southern parts of the island and they post-date the caldera collapse there.

A rhyolite dome and an associated flow are beautifully exposed in the northern sea cliff (Fig. 3). The dome is at least 30 m in height and is well-exposed for several hundred meters along the surf zone. The dome has well-developed sheeting which is roughly vertical at its presumed center and dips gently away from the center near the margins of the dome. In at least its upper eastern exposure, the dome extends into a thick domal flow which overlies a basal breccia zone about 1–2 m thick and is capped by a 5 m thick, blocky flow breccia. The total thickness of this late-stage domal flow is about 15 to 20 m. The lower part of the exposure reveals the body of the dome itself, which varies from a dense, foliated rock at the base, to a more altered, brecciated rock toward the top. The rocks of this dome are among the most extreme differentiates in the Galapagos Archipelago.

Intrusive Rocks. Dikes are exceedingly rare on Pinzon, despite continuous exposure along sea cliffs of the western coast which are cut close to the island's major eruptive center. Most of the dikes observed occur along the southwestern sea cliff section, where several cut Unit R. The dikes are relatively aphanitic, containing only sparse phenocrysts of plagioclase and olivine. Further to the south a small aphanitic dike turns into a sill where it intrudes a sequence of relatively flat-lying flows. A few more dikes are exposed along the southern and western coast.

Only one dike was found intruding Unit T. It is exposed in the well-developed northern sea-cliff section. The 0.7 m thick dike exhibits well-developed flow segregation, with aphanitic margins separated by a sharp boundary from a porphyritic interior. The segregation resembles that found in pahoehoe toes. The only dikes found cutting Unit N are feeders to the northwestern cinder cones.

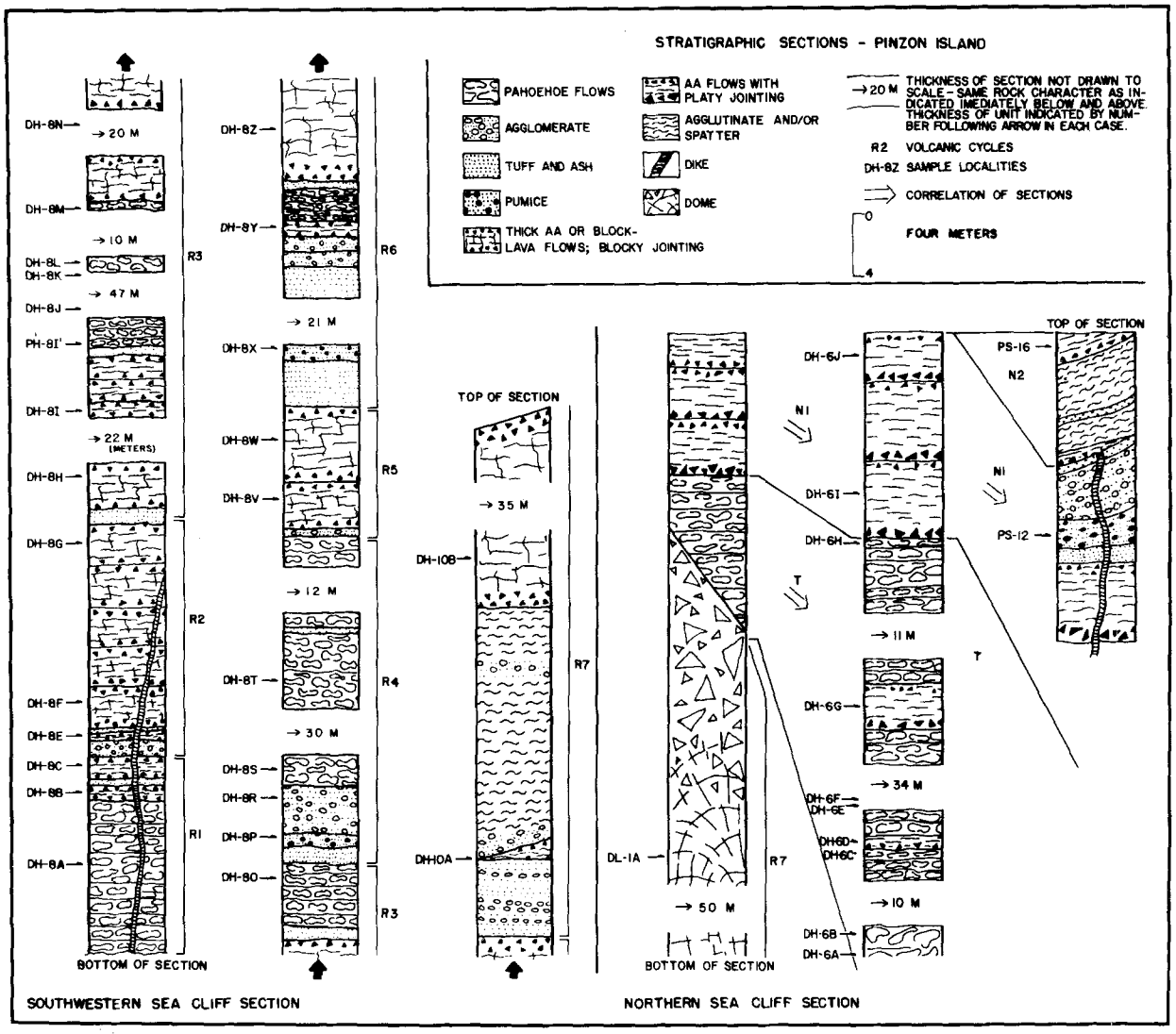

Fig. 7. Stratigraphic column showing lithologies, thickness, and sample localities. Figure 12 illustrates geochemical variation of selected major and trace elements as a function of stratigraphic height

The relative scarcity of intrusive bodies is consistent with the paucity of parasitic vents on Pinzon.

Stratigraphy

Unit R. Unit R is best exposed in the high sea-cliff sections along the southwestern side of Pinzon, but it is also exposed almost continuously around sea cliffs to a point where lavas of the younger shield coalesce with and cover lavas erupted from the southern shield. The entire southern shield is composed of flows and tuffs of Unit R, and a few reversed flows were found in the lower walls of the younger northern caldera, where flows of transitional and normal polarity visibly overlie those of reversed polarity.

All features described under 'Volcanic Features' are found in Unit R, but only a few dikes are exposed in the almost-continuous sea cliffs of the southern shield. With the exception of a single parasitic cinder cone that fed flows towards the southern coast, all reversed lavas and tephra of Unit R dip gently away from an area near the center of the southern caldera.

Because of its excellent exposures of Unit R, only the large southwestern sea cliff will be described and interpreted in detail. This cliff offers nearly 260 m of continuous vertical exposure, and the section is accessible from steep talus piles. The lavas all have reversed polarity, and K-Ar ages indicate that the entire sequence was erupted within the span of at most a few hundred thousand years (Swanson et al. 1974).

The following observations support the hypothesis that much or all of Unit R was erupted from a single central vent or localized, interconnected vents located near the older caldera: (1) No parasitic cones or other vent areas are exposed along several kilometers of continuous sea-cliff sections of Unit R; (2) there are few dikes along this portion of the sea cliff, despite its proximity to the caldera rim; and (3) the lavas and tuffs throughout the sequence have a nearly constant dip which indicates a source area located near the southern caldera.

Unit R – Volcanic Cycles. The southwestern cliff provides a continuous record of this stage of growth of the volcano. Working up the steep cliff one notes the regular appearance of interstratified

Table 1. Petrographic descriptions of analyzed samples

	Olivine basalt	Tholeiite	Plagioclase cumulate	Ferrobasalt	Icelandite	Oceanic dacite	Oceanic rhyolite
Phenocrysts							
Plagioclase	7% up to 4 mm An_{65} core to An_{55-57} rim much resorption	20%–25% up to 5 mm An_{63-70} cores to An_{45} rims euhedral	25%–55% up to 1 cm An_{65-76} cores to An_{40-45} rims disequilibrium textures	0%–25% – to 7 mm An_{52-62} cores to An_{40-45} rims some resorption	0%–30% An_{45-60} (smaller phenos – < 1 mm) larger phenos (An_{65}) show much resorption	~4% up to 1 mm An_{43-46} broken phenocrysts	~5% < 1 mm An_{15-21} equant and euhedral
Olivine	4% – up to 2 mm diam. Fo_{83-85} some brown spinel inclusions	3–8% – 0.5 mm to 2 mm diam. Fo_{68-74} often altered to iddingsite	2%–7% – 1 to 2 mm diam. Fo_{59-74}	≦2% – 0.3 mm to 1 mm diam. Fo_{57-66} some brown spinel inclusions	0–2% – < 0.5 mm diam. Fo_{50-60} but variable, $Fo_{45, 63, 72}$ in one sample, commonly altered	occasional olivine < 1 mm diam. Fo_{36-64}	occasional small microphenocrysts light green
Clinopyroxene	few% – up to 3 mm $Fs_{10}Wo_{43}En_{47}$ $Fs_{14}Wo_{42}En_{44}$ zoned	0%–3% $Fs_{15}Wo_{42}En_{44}$ $Fs_{20}Wo_{38}En_{42}$ yellow	0%–7% – up to 2 mm diam., $Fs_{17}Wo_{41}En_{42}$ (in 2), golden yellow	< 1% – to 1.5 mm diam. $Fs_{19}Wo_{40}En_{41}$ golden yellow	1–5% – 0.3 mm to 1 mm diam. $Fs_{19}Wo_{38}En_{43}$ $Fs_{20}Wo_{40}En_{40}$ golden yellow	< 1% – up to 1 mm $Fs_{27}Wo_{38}En_{35}$	< 1% to 1 mm $Fs_{47}Wo_{44}En_{9}$ $Fs_{48}Wo_{50}En_{2}$ green to brown
Orthopyroxene					~1% in one sample $Fs_{35}Wo_{4}En_{61}$	minor opx	
Oxides	occasional phenocrysts	none	occasional microphenocrysts (in one)	a few titanomagnetite phenocrysts in one sample	0%–2% – to 1 mm titanomagnetite	minor opaque microphenocrysts	occasional opaques
Groundmass	intergranular, plag. laths, clinopyroxenes, opaques, olivine	plag. laths, purple-brown cpx, opaques, minor olivine, glass (in 2)	similar to tholeiite	rich in opaques, feathery ilmenite, equant magnetite, plag. laths, light-brown cpx, minor olivine, dark brown glass	intergranular to hyaloophitic, plag. laths, cpx, opaques, minor olivine, abundant glass, occasional pigeonite, apatite	porous, pale brown glass, plag. microlites, cpx microlites	very fine-grained matte, alkali feldspars, opaques, altered mafics, apatite, zircon

light-colored tuffs which seem to represent the initiation of different cycles of activity. Light-colored tephra beds a few centimeters to 5 m thick are commonly followed by several 0.5 to 10 m aphanitic aa flows, and finally by many phenocryst-rich pahoehoe lavas. A complete sequence of these lithologies is here defined as a volcanic cycle. After a thick series of these phenocryst-rich lavas a new cycle is marked by the appearance of another tephra horizon, overlain by a sequence of lavas similar to those mentioned earlier. Some cycles are incomplete and one may find variations and exceptions to this general scheme of eruptive activity. No evidence of erosion or soil development is found between the eruptive cycles of Unit R. However, if a major time break had occurred between these units it might be difficult to detect. The lack of extensive soil development or erosion in the past several hundred thousand years following the final activity on the island indicates that long periods may elapse with little erosion or weathering.

At least seven eruptive cycles can be detected in the 260 m sea-cliff section on the basis of stratigraphic, petrographic, and compositional evidence, and are described below. A diagrammatic representation of the southwestern sea cliff section is given in Fig. 7. Compositions of tephra presented below were determined by analyses of the juvenile components of individual units.

R1 is represented by the lowermost unit, consisting of about 12 m of intertonguing pahoehoe flows. These flows are the oldest lavas exposed on Pinzon and three analyses indicate that the lavas are all ferrobasalts. The lavas are interpreted as the top of the oldest eruptive cycle exposed.

R2 is the first well-defined eruptive cycle. Units belonging to it begin with two yellow-brown icelandite tuffs and a thin interbedded aa flow. The lowermost tuff is approximately 1 m thick and contains numerous fragments of lava and gabbro. Above the tuffs are at least five aphanitic aa flows which become increasingly

Table 2. Representative analyses of silicate and oxide minerals in Pinzon lavas

Sample	DH-8M	DH-8M	DH-8J	DH-8J	DH-8B	DH-8B	DH-8H	DH-16B	DL-1A*
Plagioclase feldspar phenocrysts									
SiO_2	51.00	51.40	52.60	53.10	55.00	55.40	56.30	56.40	–
TiO_2	0.08	0.07	0.06	0.09	0.10	0.14	0.03	0.04	–
Al_2O_3	30.90	30.90	30.30	29.20	28.70	27.80	27.80	27.20	–
FeO*	0.58	0.60	0.57	0.55	0.53	0.70	0.49	0.58	–
MgO	0.15	0.15	0.13	0.13	0.12	0.10	0.06	0.08	–
CaO	13.80	13.40	12.90	12.00	11.00	10.40	10.00	9.40	2.54
Na_2O	3.42	3.74	4.15	4.49	4.92	5.36	5.90	6.20	6.99
K_2O	0.06	0.08	0.10	0.15	0.17	0.20	0.16	0.25	0.55
Total	99.99	100.34	100.81	99.71	100.54	100.10	100.74	100.15	10.08
Mole % An	69	66	63	60	56	52	47	44	$(An_{17}Or_4Ab_{79})$
DL-1A* – 3 element feldspar analysis									
Clinopyroxene phenocrysts									
SiO_2	48.00	48.00	50.40	50.80	49.70	50.50	51.00	50.60	48.24
TiO_2	2.47	2.84	1.11	0.97	1.75	1.26	0.66	0.78	0.52
Al_2O_3	4.60	5.13	2.41	1.98	2.73	2.02	1.72	1.80	0.74
FeO*	9.40	12.50	9.70	8.90	11.70	12.50	14.30	12.00	26.44
MgO	13.70	12.10	15.00	15.40	14.00	14.90	12.90	13.80	2.85
CaO	19.80	19.10	20.10	18.60	18.90	19.30	19.20	19.90	19.59
Na_2O	0.34	0.40	0.31	0.33	0.32	0.31	0.34	0.37	–
K_2O	–	–	–	–	–	–	–	–	–
Total	98.31	100.07	99.03	96.98	99.10	100.79	100.12	99.25	98.38
Mole % Fs	16	21	16	15	19	20	23	19	47
Wo	43	42	41	40	40	39	40	41	44
En	41	37	43	46	41	42	37	40	9
Olivine phenocrysts									
SiO_2	38.20	37.90	37.30	37.10	36.50	35.30	36.60	–	–
TiO_2	0.01	0.02	0.03	0.07	0.03	0.08	0.04	–	–
Al_2O_3	0.05	0.05	0.07	0.06	0.06	0.08	0.06	–	–
FeO*	23.90	24.80	27.40	27.70	29.80	37.80	35.10	–	–
MgO	37.60	37.20	35.10	34.50	32.00	26.00	29.10	–	–
CaO	0.35	0.37	0.34	0.36	0.35	0.40	0.35	–	–
Na_2O	0.02	–	0.02	0.01	0.02	0.01	0.03	–	–
K_2O	–	–	–	–	–	–	–	–	–
Total	100.13	100.34	100.26	99.80	98.76	99.67	101.28	–	–
Mole % Fo	74	73	70	69	66	55	60	–	–

Sample Spinels	DL-1A	DH-8B	DH-8H	DH-10A	DH-10A Ilmenite
SiO_2	0.59	0.25	0.05	0.03	0.01
TiO_2	23.9	26.6	22.9	17.1	49.1
Al_2O_3	0.58	1.13	2.31	1.97	–
Cr_2O_3	–	0.10	0.14	1.28	0.14
FeO*	69.5	67.9	68.7	77.1	47.8
MgO	0.05	0.33	1.24	0.67	1.21
CaO	0.17	0.03	–	–	–
Na_2O	–	0.02	–	–	–
Total	94.79	96.36	95.34	98.15	98.26

mafic and increasingly porphyritic upsection (Fig. 12). This cycle is roughly 15 m in thickness.

R3 is the most complete eruptive cycle in this section. Its units total more than 100 m in thickness starting with 1 m of aphanitic lapilli tuff of basaltic composition. This explosive eruption was followed by about 30 m of icelandite aa lavas overlain by a thick sequence of relatively phenocryst-poor pahoehoe basaltic lavas. The flows become increasingly porphyritic upsection.

R4 was initiated by deposition of several meters of tephra, which include a pumice-rich layer that is dacite in composition, and a few meters of agglomerate rich in gabbroic inclusions. Overlying the tephra beds are 50 m of porphyritic pahoehoe flows of tholeiitic basalt. Owing to inaccessibility, this cycle was not sampled in detail, but it was estimated to be nearly 60 m thick.

R5 has 0.5 m of agglomerate at its base, followed by a 3 m aphanitic aa icelandite flow which is then overlain by a 5 m aa flow of tholeiitic basalt containing nearly 50 percent plagioclase phenocrysts.

R6 has a thickness of about 40 m, of which 30 m are tephra beds. The lower part of the sequence includes pumice, tuff, and agglomerate layers, parts of which are icelandites. Overlying the tephra are aa and pahoehoe lavas of tholeiitic basalt, with a 0.5 m intercalated tuff layer.

R7, together with the domal flows inside the southern caldera, probably represents the final phases of activity of the southern central vent. Several meters of tephra, agglutinate, and spatter form the base of the sequence. A 50 m thick flow of basalt forms the bulk of R7. The flow forms a dip slope up to the rim of the southern caldera and can be traced laterally to the north, indicating the unusual thickness was not caused by ponding in an earlier collapse feature. Sometime during or slightly after the extrusion of this sequence the last major collapse of the southern caldera took place.

Following collapse of the southern caldera a thick dome and series of domal flows were extruded onto its floor, marking the end of Unit R activity.

Units T and N. Units T and N are restricted to the northern younger shield of Pinzon. They are exposed in the upper walls of the northern caldera and cover the entire surface of the younger shield.

The thickest section of transitional polarity Unit T is exposed in the large northern sea cliff where lavas at least 70 m thick flowed over and around a large rhyolite dome of Unit R (Fig. 3). These lavas consist of pahoehoe flows with little or no interbedded tephra, and only a single aa flow. Seven analyses indicate that the lavas are all ferrobasalts. Portions of the sequence exposed in the western and eastern walls of the northern caldera also have transitional polarities (Swanson et al. 1974).

Towards the top of the northern sea-cliff section there is an abrupt change that marks the base of Unit N. Here, several 1- to 3-meter thick icelandite aa flows of normal polarity overlie the ferrobasalt pahoehoe flows of transitional polarity. No evidence of erosion or soil development is found between flows of Units T and N. Unit N flows apparently extend from the younger northern caldera to the sea and cap the northernmost flanks of Pinzon. On portions of the northeastern flanks of the northern shield only a single flow of Unit N has reached the sea. It overlies the lavas of Unit T which are exposed only in cliff sections.

Thick flows of Unit N are well-exposed in the walls of the younger caldera. A 50 m thick flow exposed along a partially subsided fault block on the western margin of the caldera may represent infilling of an earlier collapse feature. Analyses of the flows of Unit N exposed in the caldera walls indicate that all are icelandites.

Development of the younger shield ended with formation of a caldera and the construction of a pair of parasitic cinder cones. A several-meter-thick tephra unit, rich in pumice lapilli and bombs, that may have been erupted during the formation of the caldera is exposed on a partially-subsided fault block on the west side of the caldera (Fig. 2). A 1- to 4-meter thick bed now buried below the pair of coalescing cinder and agglutinate cones along the northwest coast may represent the same pyroclastic event.

The construction of these cones, shown as Unit N2 in Fig. 2, marks the end of volcanic activity on Pinzon. The radial dips of beds away from points perhaps 20 to 40 m seaward from the coast indicate that only about 40% of each cone still remains. The basaltic lavas erupted from these cones are markedly different in composition from other lavas of Pinzon (analysis #PS-16, Table 3).

Petrography – Analytical Methods

Rock names have been assigned on the basis of bulk compositions. According to criteria presented by Irvine and Baragar (1971), the volcanic rocks of Pinzon belong to the typical oceanic tholeiite association, and they exhibit continuous chemical variation. The terms dacite and rhyolite as used in this paper refer to oceanic rather than continental setting. A distinct group of lavas occurs near the peak of the iron enrichment trend when plotted on an AFM diagram (Fig. 10): McBirney and Williams (1969) use the term ferrobasalt for such lavas (which contain more than 12.5% total FeO and have MgO contents of less than 6%), and this usage is adhered to here.

Approximately 200 rocks collected from Pinzon were sectioned and examined under the microscope. Detailed studies of some sections were made using universal stage techniques, and analyses of phenocrysts and some ground-mass minerals in selected samples were done by electron-beam microprobe using correction procedures similar to those of Rucklidge (1967). The brief petrographic synthesis of the main rock types, Table 1, is drawn from those rocks which have been analyzed. The X-ray fluorescence spectrometry (XRF) procedures of Norrish and Hutton (1969), with slight modifications, were used to determine the major element compositions, except for Na contents. Trace-element analyses (Lindstrom 1976) are available for numerous samples collected from Pinzon. Contents of Rb, Sr, Zr, and Ni were also determined by XRF. Contents of Na and of Sc, Cr, Co, Ba, La, Ce, Sm, Eu, Tb, Yb, Lu, Hf, Ta, and Th were determined by instrumental neutron activation analysis (INAA) using slightly modified procedures of Gordon et al. (1968).

Petrographic descriptions of major rock types are shown in Table 1 and representative analyses of silicate and oxide minerals from Pinzon lavas are given in Table 2. (Sample localities are given in Figs. 7 and 8).

Petrochemistry

Despite their minor petrographic and chemical irregularities, Pinzon lavas clearly conform to the major compositional features of tholeiitic series found on oceanic islands. The complete gradation in composition, mineralogy, and occurrence indicates that the island's lavas are serial and are probably genetically related.

Chemical analyses and molecular norms are presented in Table 3 for representative whole rock samples of lavas and tuffs from Pinzon. (Complete tables

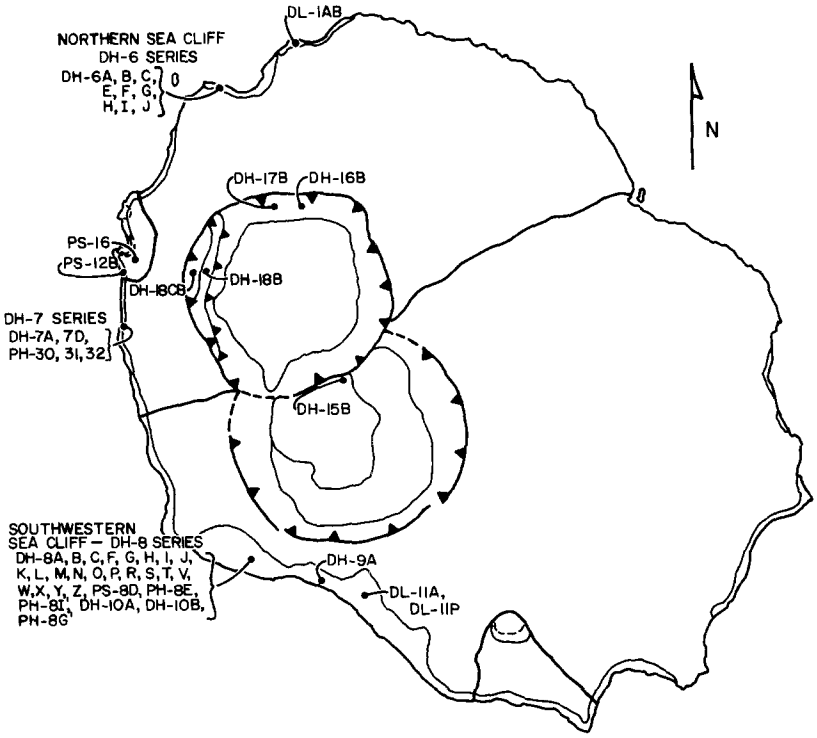

Fig. 8. Sample locality map for Pinzon Island (also see Fig. 7 for locations of samples collected from sea cliffs)

available from author upon written request). The compositional variations of the rocks are reflected in their normative minerals. Il and Mt increase to the ferrobasalts and then rapidly decline. An decreases from the basic to the acid end of the series, while Or and Ab increase. Both Di and Ol decrease rapidly, Ol being present in the tholeiitic basalts.

The basalts are all hypersthene normative and contain small amounts of either normative quartz or olivine (Table 3). The Pinzon Island basalts are saturated or oversaturated with respect to silica, and progressively differentiated rocks have increasing amounts of normative quartz. Although the oxidation state of iron is often altered in Pinzon lavas, and higher values of Fe_2O_3 tend to decrease the amounts of silica-undersaturated minerals in the norm, it can be seen that fresh lavas with low Fe_2O_3/FeO still have normative hypersthene.

Harker-type diagrams using a commonly used differentiation index, DI (Thornton and Tuttle 1960), plotted against the abundances of selected oxides and trace elements are used to illustrate the variation in Pinzon lavas (Fig. 9). Rocks on Pinzon are characterized by the following compositional variations with differentation: contents of SiO_2, alkalies, and trace elements Ba, Rb, Zr, Hf, Ta, Th, and the REE increase continuously in the series; MgO and CaO contents decrease continuously, as do those of trace elements Ni, Cr, Co, and Sr; FeO* (total iron as FeO) and TiO_2 contents reach a maximum in the ferrobasalts and then decline; and P_2O_5 contents reach a maximum in the icelandites and then decline.

High Al_2O_3 and CaO contents in Pinzon lavas can be correlated with large modal percentages of plagioclase. Several of the analyzed basalts within Unit R contain abundant phenocrysts of plagioclase, an observation which suggests accumulative addition of this mineral, a process that would diminish contents of FeO*, MgO, and other oxides which are excluded from feldspars.

Except for the more differentiated rocks, TiO_2 contents are generally in excess of 1.75%, and thus the lavas conform with Chayes' (1964) generalization for basaltic rocks of oceanic regions. As pointed out by McBirney and Williams (1969) for Galapagos rocks, TiO_2 contents vary directly with FeO* contents (Fig. 12). Pinzon ferrobasalts often contain more than 4% TiO_2 and as much as 16% FeO*.

Both K_2O and Na_2O contents increase with differentiation, but the relative increase for K_2O is much more rapid; Na_2O/K_2O decreases from 6.1 in basalts to 1.5 in the rhyolites. The transitional nature of the Pinzon Island suite is illustrated on the total alkalies-silica diagram (Fig. 11). Basaltic rocks plot on either side of the boundary between the Hawaiian alkalic and tholeiitic series (Macdonald and Katsura 1964),

Table 3. Major and trace element content of representative Pinzon lavas

Rock type	Olivine basalt	Tholeiite			Plagioclase cumulate		Ferrobasalt			Icelandite					Dacite		Rhyolite	
Sample number	PS-16	DH-8K	DH-8M	DH-8T	DH-80	DH-8Y	DH-8B	DH-6B	DH-6H	DH-17B	DH-8G	DH-6J	DH-8V	DH-8X	DH-8P	DH-8R	DL-1A	DH-18C
	Major element oxides (%)																	
SiO_2	47.85	48.24	47.97	48.52	48.12	48.42	48.84	48.26	46.63	53.48	51.02	54.70	53.44	58.83	62.20	62.74	69.77	68.19
TiO_2	1.78	2.49	2.71	2.59	2.08	1.68	3.40	3.61	4.40	2.13	2.86	2.06	2.49	1.29	0.89	0.96	0.38	0.27
Al_2O_3	15.79	14.93	14.66	15.76	17.86	20.24	13.27	15.22	11.93	15.24	13.90	14.97	14.04	15.72	14.75	14.72	13.19	12.84
Fe_2O_3	6.13	4.06	2.73	5.72	3.30	4.97	4.30	3.88	5.57	3.81	8.17	2.71	5.10	2.27	1.40	3.26	2.14	1.96
FeO	5.05	8.72	10.20	7.31	7.04	3.74	10.59	9.55	10.66	6.94	5.03	7.79	7.12	4.91	4.32	2.57	3.14	2.13
MnO	0.19	0.19	0.21	0.20	0.16	0.13	0.23	0.20	0.25	0.17	0.22	0.21	0.22	0.14	0.13	0.13	0.16	0.13
MgO	7.86	6.78	6.44	5.58	6.10	4.48	4.87	4.31	4.70	4.11	4.34	4.01	3.45	2.65	1.51	1.44	0.05	0.14
CaO	11.37	10.39	10.91	10.27	11.56	12.13	9.15	10.07	9.97	8.14	7.97	7.96	7.17	5.57	3.51	3.69	1.60	1.31
Na_2O	2.56	2.93	2.90	2.95	2.81	2.74	3.23	3.21	3.23	3.44	3.70	3.87	3.95	4.51	5.15	5.21	5.80	5.05
K_2O	0.27	0.43	0.40	0.42	0.36	0.28	0.62	0.69	0.81	1.01	1.13	1.08	1.08	1.49	2.09	2.04	2.98	4.05
P_2O_5	0.28	0.27	0.28	0.31	0.24	0.20	0.41	0.38	0.50	0.31	0.58	0.31	0.71	0.31	0.27	0.26	0.04	0.05
Loss	0.23	0.30	0.29	0.75	0.30	0.46	0.79	0.06	0.48	0.58	1.07	0.45	1.02	2.55	3.77	1.56	0.25	3.74
Total	99.34	99.72	99.70	100.37	99.92	99.46	99.71	99.44	99.12	99.35	99.99	100.12	99.80	100.23	99.97	98.58	99.50	99.86
	Molecular norms																	
ap	0.60	0.58	0.60	0.66	0.51	0.43	0.89	0.82	1.10	0.67	1.26	0.66	1.54	0.67	0.59	0.56	0.09	0.11
il	2.52	3.54	3.86	3.69	2.93	2.38	4.93	5.19	6.44	3.05	4.13	2.92	3.59	1.85	1.29	1.38	0.54	0.39
or	1.62	2.59	2.41	2.54	2.15	1.68	3.81	4.21	5.03	6.14	6.92	6.48	6.60	9.04	12.83	12.45	17.79	24.96
ab	23.36	26.82	26.60	27.12	25.50	25.05	30.17	29.74	30.48	31.78	34.42	35.30	36.71	41.61	48.04	48.31	52.63	47.30
an	31.30	26.83	26.36	29.20	35.44	42.88	20.68	25.89	16.46	23.83	18.63	20.61	18.00	18.75	11.39	11.11	1.17	0.42
mt	6.51	4.33	2.92	6.12	3.49	5.29	4.68	4.19	6.12	4.10	6.46	2.88	5.52	2.44	1.52	3.52	2.26	2.14
hm	0.0	0.0	0.0	0.0	0.0	0.0	0.0	0.0	0.0	0.0	1.60	0.0	0.0	0.0	0.0	0.0	0.0	0.0
di	19.34	19.14	21.65	16.71	16.76	13.66	19.01	18.49	25.68	12.51	14.73	13.96	11.22	6.05	3.90	4.84	5.27	4.48
hy	13.78	13.23	8.41	11.56	8.94	5.96	13.88	10.65	8.05	10.97	5.05	12.03	8.76	9.06	7.24	2.28	0.63	0.0
ol	0.0	2.95	7.20	0.0	4.30	0.0	0.0	0.0	0.0	0.0	0.0	0.0	0.0	0.0	0.0	0.0	0.0	0.0
q	0.97	0.0	0.0	2.40	0.0	2.66	1.95	0.83	0.64	6.94	6.81	5.16	8.06	10.54	13.21	15.56	19.63	20.04
	Trace elements (ppm)																	
Ni	160.	93.	70.	57.	–	54.	–	–	–	36.	13.	42.	–	–	–	–	–	–
Co	47.3	49.3	46.5	44.2	38.5	34.2	43.0	37.9	45.0	29.5	33.0	32.0	30.3	16.9	8.2	8.0	0.73	0.58
Sc	32.4	33.2	34.5	32.5	27.2	25.2	35.0	29.9	40.3	27.7	28.2	26.0	25.1	13.9	12.1	11.9	4.5	2.0
Cr	292.	60.	70.	50.	66.	57.	28.	28.	35.	88.	15.	71.	7.2	10.3	–	2.5	4.4	–
Ba	–	80.	–	80.	35.0	–	110.	–	160.	150.	160.	170.	215.	230.	320.	300.	425.	475.
Sr	276.	320.	318.	324.	349.	384.	288.	–	273.	261.	296.	270.	282.	258.	194.	198.	91.	64.
Rb	< 5.	6.	8.	9.	5.	6.	12.	–	12.	18.	21.	23.	26.	29.	43.	34.	54.	67.
Ta	0.71	1.05	1.09	1.20	0.75	0.83	1.56	1.63	2.09	1.73	2.13	1.99	2.67	2.02	2.75	2.50	6.1	5.6
Hf	3.00	3.8	4.0	4.3	2.9	3.0	6.0	5.8	7.6	8.4	8.1	9.0	10.7	10.7	14.7	13.5	25.7	23.5
Zr	128.	157.	171.	177.	131.	120.	249.	–	294.	323.	344.	396.	453.	433.	617.	575.	1,032.	876.
Th	0.78	1.15	1.15	1.30	0.88	0.86	2.03	1.77	2.37	3.59	3.00	3.36	4.09	5.45	7.10	7.05	9.3	10.6
La	8.9	12.0	13.0	13.3	8.7	9.8	18.5	16.8	22.3	25.7	25.9	27.1	34.	30.5	41.	37.	70.	70.
Ce	23.	29.	30.	32.	22.	23.	44.	40.	56.	62.	61.	63.	84.	74.	100.	87.	146.	153.
Sm	4.08	5.1	5.2	5.7	3.8	4.0	8.4	7.7	9.4	9.6	10.1	10.6	12.8	8.8	11.7	11.9	21.5	22.0
Eu	1.54	1.89	1.96	2.13	1.54	1.55	2.65	2.56	3.20	2.77	3.19	2.75	3.65	2.46	2.88	3.10	4.41	3.81
Tb	0.70	0.95	1.04	1.09	0.71	0.71	1.46	1.21	1.82	1.63	1.77	1.82	2.23	1.54	2.06	1.95	3.92	3.94
Yb	2.25	2.6	2.6	3.0	1.89	2.0	4.0	3.4	4.7	4.5	4.8	5.3	6.2	4.81	6.4	6.0	13.0	12.9
Lu	0.35	0.43	0.35	0.41	0.29	0.24	0.55	0.52	0.65	0.72	0.77	0.80	0.83	0.80	1.00	0.95	1.79	1.81
Differentiation index	25.95	29.41	29.01	32.05	27.65	29.40	33.39	34.78	36.15	44.86	45.58	46.94	51.38	61.19	74.07	76.31	90.05	92.29

but the differentiated rocks lie on the tholeiitic side of the line.

In an AFM diagram, compositions of Pinzon lavas define a strong trend of iron enrichment and then depletion, coupled with continuous strong enrichment of alkalies (Fig. 10). Among the more basic rocks there is a pronounced trend toward increasing FeO*/MgO with little increase in alkali contents. This trend is quite similar to that exhibited by the tholeiitic lavas of Thingmuli, Iceland (Carmichael 1964).

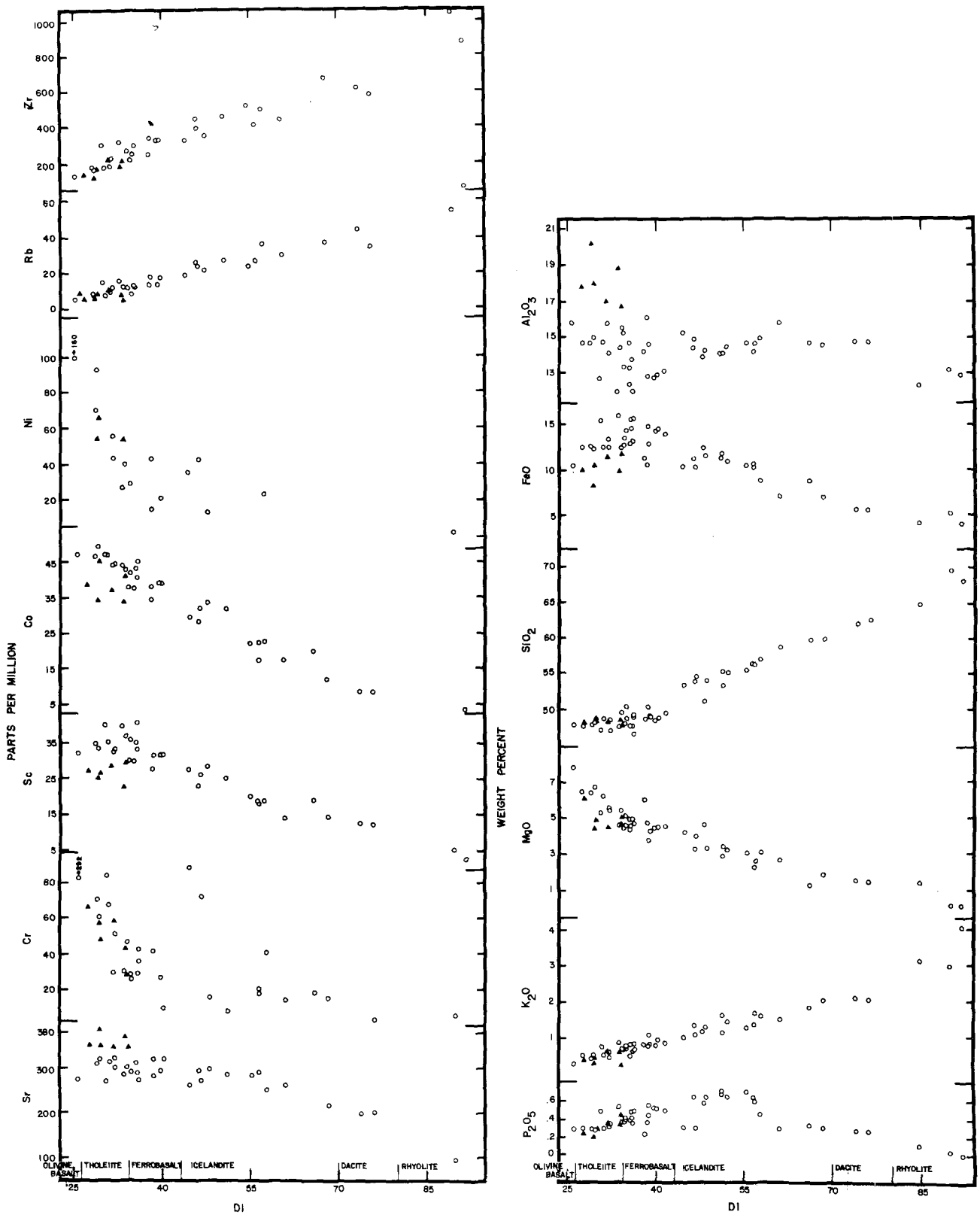

Fig. 9. Variation diagrams for selected major and trace elements in Pinzon lavas as a function of the Thornton-Tuttle Differentiation Index (*DI*); *FeO:* total iron as ferrous iron; ▲-plagioclase cumulates

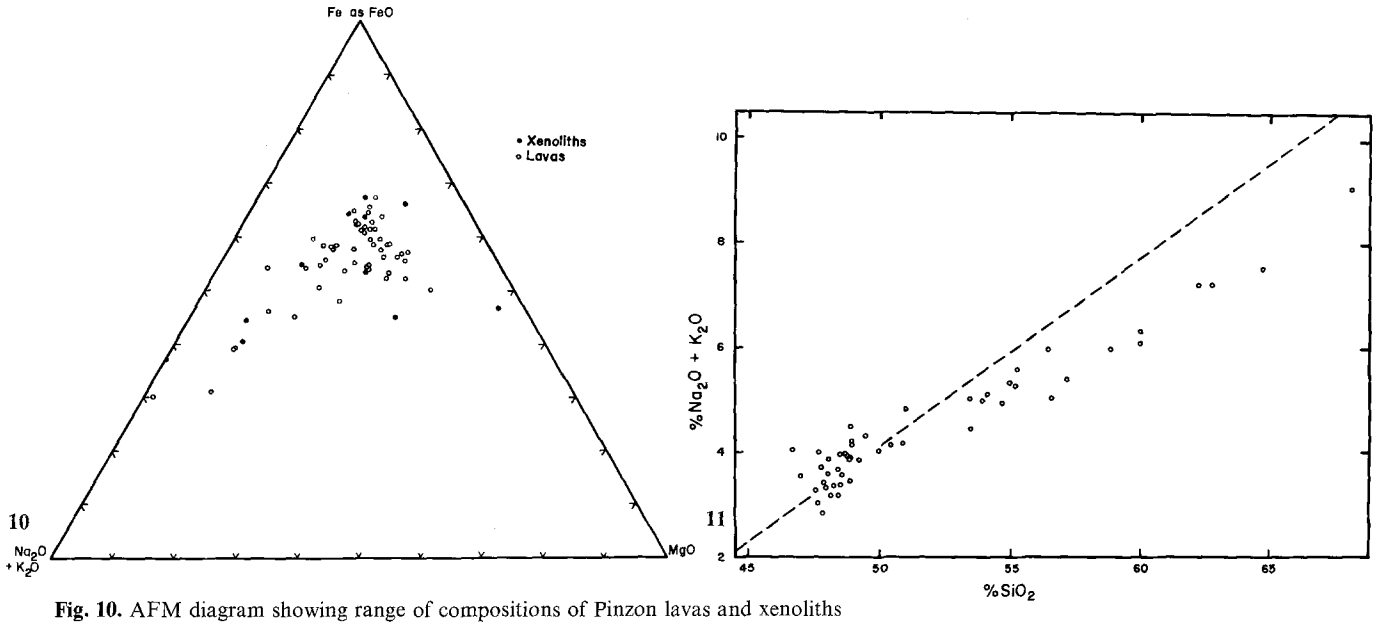

Fig. 10. AFM diagram showing range of compositions of Pinzon lavas and xenoliths

Fig. 11. Total alkalies-silica diagram for Pinzon lavas. *Dashed line* separates the Hawaiian tholeiitic from alkali basalts (Macdonald and Katsura 1964)

Geochemical Variation – Stratigraphic Considerations

As discussed earlier, the stratigraphic succession of the lavas of Pinzon can be divided into several units; R, T, and N. Although the corresponding three periods of igneous activity can be distinguished in space and time, they are not necessarily represented by lavas with different geochemical characteristics.

Geochemical variations among 43 samples representing the oldest to youngest eruptive rocks involved in the construction of Pinzon are presented in Fig. 12. A corresponding stratigraphic column showing sample locations is given in Fig. 7. A brief summary of the geochemical characteristics of rocks of each unit follows:

1. Unit R consists of 7 eruptive cycles exposed in the southwestern sea cliff. These subdivisions are also evident in the geochemical trends through the history of Unit R. The lowermost cycle is not as well-defined as the others, probably because the three samples assigned to it represent only the upper portion of an eruptive cycle. Cycle R2 is based on only three samples. A fourth sample was analyzed but was not plotted on Fig. 12 because it showed evidence of major post-depositional alteration. This sample is from light-colored tuff at the base of the cycle and was probably an icelandite. Cycles R2, R3, R4, R5, and R6 all were initiated by tephras of relatively siliceous composition, and within each of the last four cycles there are trends toward more mafic compositions upsection (Fig. 12). Cycle R7 was initiated by an agglomerate (no analysis was made), and two samples (DH-10A and DH-10B) represent later lavas of this cycle exposed near the top of the southwestern sea cliff. Samples DH-15 and DL-1 are included in cycle R7, although they may not correlate directly with any definite cycle (DL-1 is the only eruptive unit with a reversed polarity exposed in the northern sea cliffs, and DH-15 definitely postdates DH-10B because it is from a domal flow of reversed polarity which was extruded after collapse of the large southern caldera).

2. Lavas of transitional polarity (Unit T) are more than 70 m thick in the northern sea cliff of Pinzon and consist of numerous uniform ferrobasalt flows which are distinguished by high FeO*, TiO_2, and Sc contents (Fig. 12). This uniformity is unlike Unit R, which is characterized by diverse styles of eruptive activity (including explosive activity) and wide varieties of rock compositions and lithologies. Hence the shift in eruptive centers (from the southern caldera to the northern caldera) correlates with a change in the nature of volcanism.

3. Unit N can be subdivided into two subunits: Unit N1 and Unit N2. Unit N1 is distinctive in that it consists of more-differentiated rocks (icelandites and rhyolites) and contains no true basalts. Except for two samples, icelandites of Unit N1 are compositionally indistinguishable from those of Unit R. However, two samples were found to contain markedly higher Ni and Cr contents and lower P_2O_5 contents than do the other icelandites. A small amount of

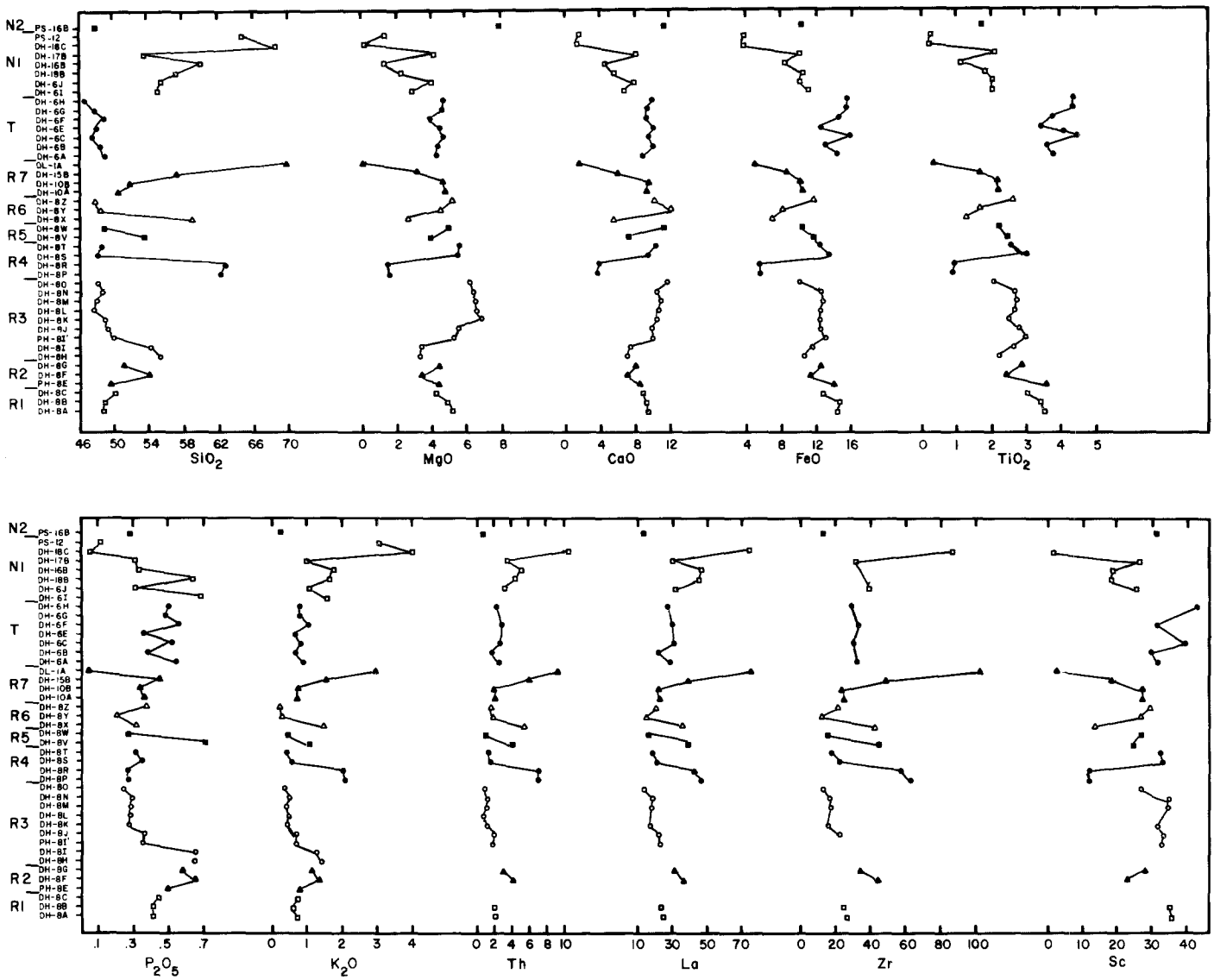

Fig. 12. Geochemical variation of selected major and trace elements as a function of stratigraphic height. Refer to Figs. 7 and 8 for sample locations

rhyolite pumice represents the final eruptive phase of Unit N1.

Unit N2 represents the final activity on Pinzon, and a representative sample indicates that the parasitic cones located on the northwestern tip of the island are composed of a basalt characterized by unusually low contents of alkalies, TiO_2, FeO*, and excluded trace elements, but significantly higher contents of MgO, Cr, and Ni than those of other lavas of the island.

The eruption of some of the major units from different centers poses questions as to possible relationships between lavas. The eruptive styles and observed compositional sequences present interesting questions about the eruptive mechanisms of volcanoes and the differentiation process involved in the evolution of Pinzon magmas. These questions are discussed below.

Petrogenesis

Geologic Model

Several lines of evidence suggest that most of the Pinzon lavas are genetically related through fractional crystallization of a series of magmas of common parentage. From the geological relations, it is apparent that the lavas are closely related in space and time. The lavas contain similar mineral phases and exhibit

a continuum of changing compositions with differentiation. A comparable variation is found in accidental gabbroic xenoliths, which contain mineral phases like those of the lavas. Geochemical analyses indicate that the lavas lie on relatively smooth trends of variation diagrams (with only a few exceptions which will be discussed later), and that most compositions probably represent points along a liquid line of descent.

The cycles of Unit R can best be explained by crystal fractionation and appear to have been erupted from a single vent or localized, interconnected vents. Typically the base of a cycle starts with an icelandite or dacite tuff, followed by aphanitic and often glassy icelandite flows that are generally phenocryst-free. These rocks contain only occasional phenocrysts of plagioclase, yellow clinopyroxene, rare olivine, and microphenocrysts of titanomagnetite. After a series of aphanitic flows, phenocryst-rich lavas become dominant. Plagioclase phenocrysts account for more than 50% of some flows. Olivine also increases in abundance (to more than 5% in some porphyritic flows), and clinopyroxenes are also common phenocrysts, although rarely amounting to more than a few percent of the rock. Arguments follow that suggest that the phenocryst-rich lavas with very abundant plagioclase are cumulate in origin; those with less abundant plagioclase are tholeiitic basalts. Ferrobasalts, when present, usually occur between the aphanitic icelandites and the porphyritic basalts, and typically contain lesser amounts of plagioclase, olivine, and clinopyroxene phenocrysts than do the overlying lavas. The gradational compositions of rocks of these eruptive cycles are illustrated in Fig. 12.

The stratigraphic, petrographic, and major-element compositional features of such cycles can be best explained as the consequence of tapping a compositionally-zoned magma chamber that had undergone fairly extensive crystal fractionation. The following is a crude, generalized model that may best explain the observed geological and compositional features of an ideal cycle.

Following intrusion of a body of magma to shallow depths beneath the major volcano of Pinzon, convection may have brought fresh hot magma to the top of the reservoir while simultaneously removing cooled basaltic magma somewhat depleted in volatile components to the bottom. The relatively low density and high viscosity of the upper material may then have prevented it from being carried downward by convection. As cooling and crystallization progressed within the shallow part of the reservoir, visualized as a simple chamber, volatile components could have been exsolved until gas pressures exceeded the pressure of the overlying rock column. At that point explosive activity began and the associated release of pressure resulted in further exsolution of volatiles to maintain the eruption. In this manner, light differentiates at the top of the magma body were explosively erupted to form pyroclastic deposits. As an individual cycle progressed, magma was drawn from successively deeper levels of the reservoir, and the less differentiated and more voluminous lavas could passively rise to the surface. The resulting tuff-flow stratigraphy would, therefore, be the inverse of the original zonation of the magma column.

The volcanic cycles and their associated rock types repeat fairly systematically. The cyclical patterns are almost as similar in contents of trace elements as they are in contents of major elements. The resurgence of similar basaltic material (and more evolved magmas) at different stages in the volcanic sequence indicates that new material introduced into the magmatic cycles was of a similar nature on each occasion.

In light of the constraints imposed by the combined geologic-stratigraphic, petrographic, and compositional features of the lavas, models relying on processes such as magma mixing, different degrees and depths of partial melting, and assimilation are inadequate. Several lines of evidence indicate that crystal fractionation processes best explain the observed features. This generalized model is tested in the following section.

Fractional Crystallization

Major Element Tests. If similar crystal-liquid fractionation processes operated on several discrete batches of magma in relatively shallow magma chambers beneath Pinzon, then calculations in which one removes combinations of phenocrysts in various amounts from one lava should show whether it is possible to derive compositions of other lavas along a liquid line of descent. This possibility was tested by using a least-squares mixing computer program, modified from that of Bryan, Finger, and Chayes (1969), to determine the proportions of phenocrysts that must be removed to derive differentiated liquids from a given parental magma.

Mixing calculations for a sequence of lavas can be carried out in incremental steps or in cumulative steps beginning with the same parent. Incremental step calculations (going from parent lava A to derivative lava B, then from derivative lava B to more evolved lava C, etc.) resulted in consistently smaller values of the sum of the squared residuals (Σr_i^2, where r_i is the difference between calculated and observed values for each oxide) which indicates the 'goodness of fit', low values of Σr_i^2 in the range of 0 to 2 being good mathematical solutions. Cumulative mixes (go-

Table 4. Major element fractionation models

Fractionation step	F	X_{ol}	X_{plag}	X_{cpx}	X_{timt}	X_{ap}	Σr_i^2	Minerals
8K–8N	0.9411	0.0252	0.0323	0.0058	0.0016	0.0001	0.083	$Fo_{74}An_{69}Fs_{16}$Timt Apat
8K–8S	0.7390	0.0508	0.1374	0.0701	0.0042	0.0002	0.235	$Fo_{74}An_{69}Fs_{16}$Timt Apat
8K–8J	0.6727	0.0641	0.1796	0.0649	0.0173	0.0005	0.657	$Fo_{70}An_{69}Fs_{16}$Timt Apat
8K–8B	0.6718	0.0682	0.1936	0.0801	0.0006	−0.0003	0.199	$Fo_{70}An_{63}Fs_{16}$Timt Apat
8B–8E	0.8092	0.0220	0.0773	0.0588	0.0192	−0.0001	0.652	$Fo_{65}An_{63}Fs_{16}$Timt Apat
8B–17	0.7079	0.0273	0.0917	0.0867	0.0688	0.0046	1.84	$Fo_{65}An_{57}Fs_{16}$Timt Apat
8B–8G	0.7054	0.0236	0.1077	0.1039	0.0468	0.0005	0.963	$Fo_{60}An_{52}Fs_{16}$Timt Apat
8B–6J	0.5811	0.0325	0.1552	0.1283	0.0768	0.0052	0.440	$Fo_{55}An_{52}Fs_{19}$Timt Apat
8B–8V	0.4862	0.0351	0.2175	0.1670	0.0724	0.0015	0.779	$Fo_{55}An_{52}Fs_{19}$Timt Apat
8V–8F	0.9310	0.0113	0.0270	0.0148	0.0095	0.0020	0.196	$Fo_{55}An_{52}Fs_{19}$Timt Apat
8V–8H	0.9292	0.0126	0.0322	0.0144	0.0159	0.0023	0.821	$Fo_{55}An_{52}Fs_{19}$Timt Apat
8V–PH31	0.9279	0.0020	0.0029	0.0456	0.0140	0.0016	0.836	$Fo_{55}An_{52}Fs_{19}$Timt Apat
8V–7D	0.8381	0.0143	0.0424	0.0590	0.0270	0.0045	0.203	$Fo_{55}An_{52}Fs_{19}$Timt Apat
8V–6I	0.8280	0.0215	0.1006	0.0266	0.0227	0.0031	0.718	$Fo_{55}An_{52}Fs_{19}$Timt Apat
8V–8X	0.7979	0.0205	0.0605	0.0650	0.0564	0.0120	1.25	$Fo_{55}An_{52}Fs_{19}$Timt Apat
8V–1S	0.7964	0.0204	0.1049	0.0376	0.0433	0.0088	2.092	$Fo_{55}An_{52}Fs_{19}$Timt Apat
8V–18BA	0.7398	0.0295	0.1548	0.0603	0.0327	0.0048	3.86	$Fo_{55}An_{52}Fs_{19}$Timt Apat
8V–16B	0.6622	0.0337	0.1464	0.1127	0.0526	0.0108	2.703	$Fo_{55}An_{52}Fs_{19}$Timt Apat
8V–PH32	0.6188	0.0381	0.1880	0.0997	0.0622	0.0125	1.218	$Fo_{55}An_{52}Fs_{19}$Timt Apat
8V–8R	0.5712	0.0474	0.1719	0.1276	0.0639	0.0134	0.489	$Fo_{55}An_{47}Fs_{21}$Timt Apat
8V–8P	0.5695	0.0437	0.1749	0.1324	0.0650	0.0134	0.400	$Fo_{55}An_{47}Fs_{21}$Timt Apat
8P–12B	0.6291	0.0030	0.2915	0.0634	0.0217	0.0052	1.748	$Fo_{40}An_{17}Fs_{21}$Timt Apat
8P–1A	0.5919	0.0121	0.2403	0.0928	0.0133	0.0052	0.318	$Fo_{40}An_{17}Fs_{21}$Timt Apat
8P–18C	0.5079	0.0218	0.3247	0.0871	0.0185	0.0057	3.199	$Fo_{40}An_{17}Fs_{21}$Timt Apat

The fractionation step gives the parent and the daughter. F is the fraction of the parent remaining liquid. The next five columns are the weight fractions of minerals crystallized from the assumed parent in order to obtain the observed daughter. Σr_i^2 is the sum of the squares of the residuals (r_i = difference between calculated and observed values for each oxide). The last column indicates the mineral compositions used in individual fractionation steps

ing from parent A to derivative lava B, then from A to more evolved lava C, etc.) have the advantage of maintaining a consistency between different sets of calculations. However, cumulative calculations tend to be unrealistic for a wide composition range. Consequently, combinations of cumulative and incremental calculations were carried out for the Pinzon lavas (Table 4).

Sample DH-8K is one of the early lavas erupted on Pinzon, and because it is the most 'primitive' lava (i.e., has low contents of excluded elements, highest MgO content, etc.) on Pinzon, with the exception of sample PS-16, it was chosen as an assumed parental liquid for the cumulative fractionation model. Sample PS-16 was rejected as a model parent because of its unique composition, which suggests that it may not be related to the major Pinzon series. The selection of DH-8K does not imply that the sample represents a primary liquid (derived by direct partial melting of the mantle), but merely that it may serve as a reference point along the liquid line of descent of the Pinzon parental magma.

The incremental and cumulative fractionation steps used for the Pinzon lavas are summarized in Table 4. The results of the calculations are illustrated in a cumulative crystallization diagram (Fig. 13), where the proportions of separated phenocrysts are plotted against the amount of liquid remaining (F) at the stage represented by each sample. Compositions of phases fractionated were selected on the basis of their occurrence as phenocrysts and microphenocrysts in the lavas (Table 2. Table of additional compositions used is available from author upon written request). K_2O and P_2O_5 abundances were assumed to be negligible (0.01%) where not listed in Table 2. FeO* was recalculated to Fe_2O_3 for calculations. Figure 14 shows more clearly the proportions of the different phases fractionated at various degrees of fractionation.

Examination of Figs. 13 and 14 illustrates several features that are in accord with petrographic observations and the major element compositions of the lavas. The differences between the tholeiitic basalts can be explained by fractionation of plagioclase, olivine, and clinopyroxene. (The three tholeiites, DH-8L, DH-8M, and DH-8T, require minor addition and/or subtraction of these phases in order to achieve a composition like that of DH-8K). Several plagioclase-phyric tholeiites are interpreted to be of possible cumulate origin and are not discussed further here. Through-

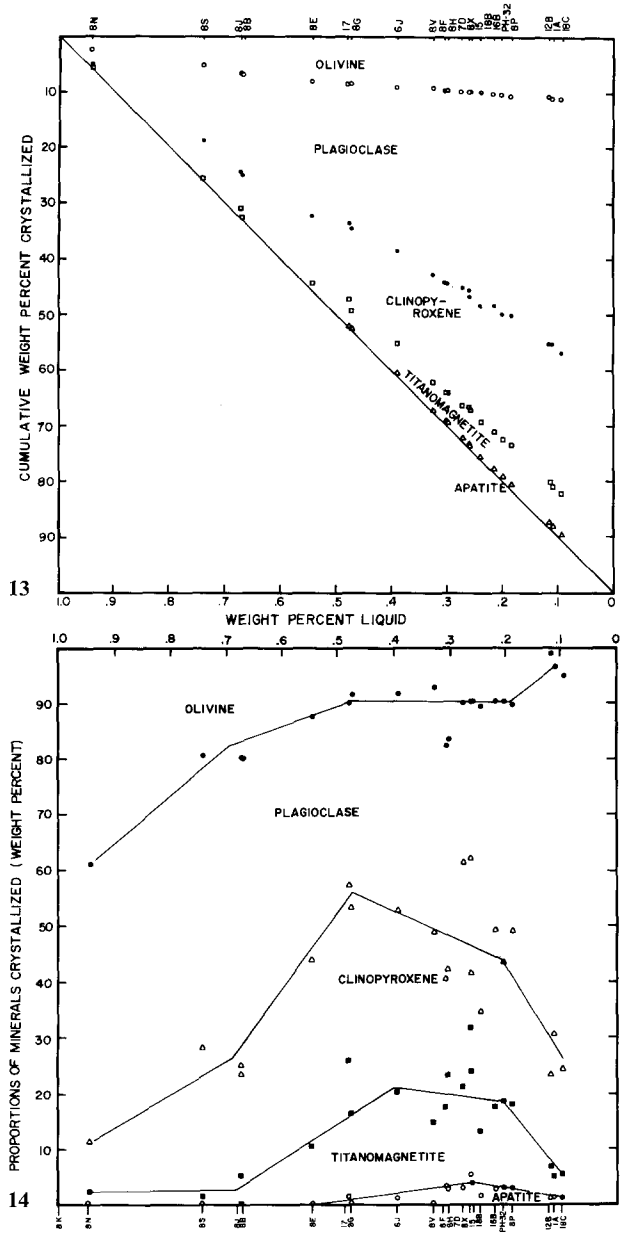

Fig. 13. Cumulative percent of phases fractionated from a parental magma assumed identical to basalt DH-8K to produce the various differentiated rocks as determined by major element mixing model calculations (see Table 4 and text)

Fig. 14. Proportions of phases fractionated from parental magma of each successive step in the scheme

out the fractionation scheme, the proportion of olivine fractionated tends to decrease. The proportion of clinopyroxene fractionated is relatively low in the early stage, increases to nearly equal proportions with olivine for the most evolved tholeiites and ferrobasalts, continues to increase through the early icelandites, but around 0.3F begins to decline. The proportion of plagioclase feldspar remains high and relatively constant except for an abrupt increase going from the oceanic dacites to the rhyolites. Fractionation of oxide minerals is minor through the early ferrobasalts, reaches a maximum in the early icelandites, and then gradually declines with increasing differentiation. Apatite fractionation, although volumetrically less important, reaches a maximum somewhat later than does titanomagnetite fractionation, and also declines in the more evolved lavas.

These results are in accord with petrographic observations which show the continual dominance of plagioclase phenocrysts, the decreasing proportion of olivine relative to clinopyroxene, and the late onset of opaque and apatite fractionation in going from basic to more evolved lavas. Compositions of phenocryst phases used in the empirically derived fractionation model were made to agree with those of observed phenocrysts at the various stages of the presumed differentiation sequence, but no constraint was put on the proportions of phases fractionated. The agreement between predictions of the model and phenocryst proportions in the rocks supports the possible relation of Pinzon lavas to a common parent by fractional crystallization. Figure 13 indicates that the final differentiates of Pinzon magmas correspond to solidification of about 90% of a magma equivalent in composition to assumed parent DH-8K. The behavior of trace elements with differentiation can provide a further test of the fractional crystallization model suggested by the major element mixing calculations.

Trace Element Tests. The distribution and fractionation of REE yield significant petrogenetic information. Numerous samples collected from Pinzon have been analyzed for several REE (Lindstrom 1976). The results, normalized to average chondritic values (Haskin et al. 1968), are compared in Fig. 15. The REE data illustrate the slightly fractionated nature of these rocks which fall in the range of many oceanic island tholeiites and are slightly enriched in the light REE relative to the heavy REE when compared to chondrites. In passing from basalts through the more differentiated rocks, there is a progressive increase in total REE abundances, but this is accompanied by only a slight relative fractionation of lighter REE (Fig. 15). The trends are consistent with the hypothesis that the rocks are related by some mechanism to a common parent.

The tholeiitic basalts of Pinzon are of two types. Several lavas with abundant plagioclase phenocrysts are probably cumulates and exhibit noticeable positive Eu anomalies (Fig. 16). Less porphyritic basalts (e.g., DH-8K, DH-8M, and DH-8N) exhibit REE patterns characterized by no or only slight Eu anoma-

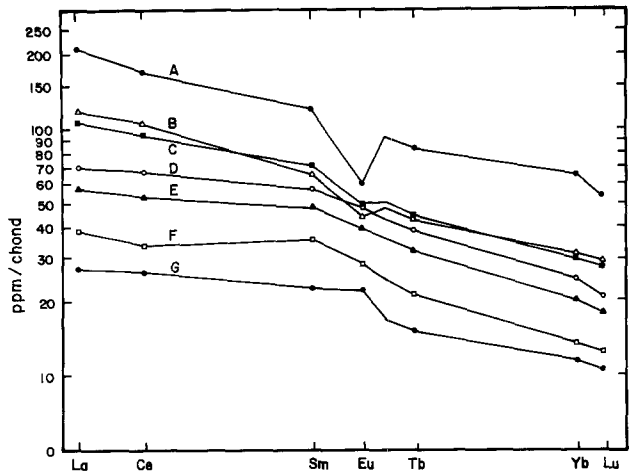

Fig. 15. REE plots of representative average analyses of Pinzon basalts and differentiates. *A* (rhyolite), average of DH-18C and DL-1A; *B* (dacite), average of DH-8P and DH-8R; *C* (icelandite), average of DH-8X, DH-8F, DH-8V, DH-15, DH-16B, DH-18B, DH-6J, PH-31, and PH-32; *D* (north coast ferrobasalts), average of DH-6A, DH-6C, DH-6H, and DH-6F; *E* (southwestern coast ferrobasalts), average of DH-8A and DH-8B; *F* (tholeiitic basalt), average of DH-8K, DH-8M, and DH-8N; *G* (olivine basalt), sample PS-16

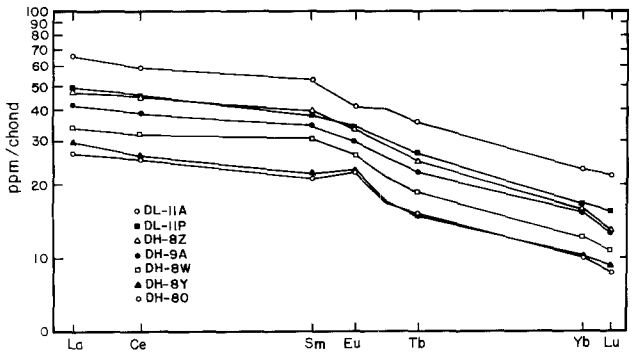

Fig. 16. REE plots of plagioclase cumulate lavas of Pinzon. DL-11A and DL-11P represent aphanitic and porphyritic portions of the same flow respectively

lies. With differentiation the REE pattern is characterized by an increasingly negative Eu anomaly (for icelandites through dacites) to a very pronounced negative anomaly for the two rhyolites, indicating that differentiation involved large amounts of minerals that selectively incorporate Eu (Fig. 15). Feldspars are practically the only minerals displaying a sharp positive Eu anomaly. Olivine extraction does not change the relative REE pattern, and plagioclase extraction does not appreciably affect the proportions of the REE other than Eu (Schilling 1971), but the magnitude of the Eu anomaly puts some stringent limits on the extent of extraction of plagioclase. However, clinopyroxenes may enrich the light REE and fractionate them appreciably, depending on the extent

Table 5. Partition coefficients used in trace element fractionation models

Element	Oliv/L	Plag/L	Cpx/L	Mt/L	Apat/L
La	0.01	0.15	0.07	0.01	10.0
Ce	0.01	0.10	0.10	0.01	18.0
Sm	0.01	0.07	0.26	0.01	29.0
Eu	0.01	0.50	0.23	0.01	20.0
Tb	0.01	0.05	0.30	0.01	26.0
Yb	0.01	0.03	0.29	0.01	13.0
Lu	0.01	0.03	0.28	0.01	11.0
Sc	0.50	0.01	3.5	2.0	0.01
Co	2.5	0.01	1.0	5.0	0.01
Cr	0.50	0.01	10.0	5.0	0.01
Ni	10.0	0.01	2.0	5.0	0.01
Ta	0.01	0.01	0.50	5.0	0.10
Zr	0.01	0.01	0.50	2.0	0.10
Hf	0.01	0.01	0.50	2.0	0.10
Th	0.01	0.01	0.01	0.01	0.10
Rb	0.01	0.20	0.01	0.01	0.01
Sr	0.01	1.7	0.15	0.01	2.0

Partition coefficient data obtained from Leeman (1974) and Lindstrom (1976) who give more specific references

of clinopyroxene loss. The heavy REE are also fractionated and enriched by clinopyroxene loss, but to a much smaller degree. Fractionation of higher pressure assemblages such as garnet and clinopyroxene would rapidly change proportions of the light REE; hence, this process could not have been important in generating the relative REE patterns of Pinzon lavas, which essentially remain the same with differentiation. Fractionation of assemblages involving predominantly plagioclase, with lesser clinopyroxene, olivine, and titanomagnetite, appears to be consistent with the REE patterns observed.

If the proportions of phases fractionated are known, and if mineral-liquid distribution coefficients are known or can be estimated, then it is possible to calculate how much of each trace element is added to or subtracted from a parent magma by fractional crystallization to produce a more differentiated liquid. General agreement between calculated and observed trace element abundances in differentiated magmas would provide support for the fractional crystallization model. Variations in the included element abundances are useful in evaluating the amounts and proportions of phases subtracted, whereas those of the excluded elements can test the total degree of fractionation.

Variations of mineral/liquid distribution coefficients with changing pressure, temperature, and bulk composition are incompletely understood. Mineral/liquid distribution coefficients show wide ranges of variation even within limited rock compositions, and there is uncertainty regarding the applicability of dis-

Table 6. Calculated and observed trace element abundances for various fractionation steps

Fractionation step	Calc. PS16/8K	Obs. 8K	Calc. 8K/8S	Obs. 8S	Calc 8K/8B	Obs. 8B	Calc. 8B/DH-17	Obs. DH-17	Calc. 8B/8G	Obs. 8G
Res. Liq.	0.636		0.738		0.657		0.720		0.716	
Ol	0.064		0.051		0.068		0.027		0.024	
Pl	0.199		0.137		0.194		0.092		0.108	
Cpx	0.090		0.070		0.080		0.087		0.104	
Mt	0.000		0.004		0.001		0.069		0.047	
Ap	0.003		0.000		0.000		0.005		0.001	
Temp.	1,225.0		1,200.0		1,175.0		1,125.0		1,125.0	
Log f_{O_2}	−8.0		−8.5		−8.5		−9.5		−9.5	
La	12.8	12.	15.7	15.7	17.3	18.5	23.4	25.7	24.5	25.9
Ce	32.4	29.	38.2	39.	42.3	44.	53.5	62.	58.3	61.
Sm	5.5	5.1	6.7	6.5	7.4	8.4	9.5	9.6	10.9	10.1
Eu	1.9	1.9	2.3	2.4	2.5	2.65	3.	2.77	3.26	3.19
Tb	0.95	0.95	1.25	1.21	1.39	1.46	1.68	1.63	1.89	1.77
Yb	3.23	2.6	3.4	3.3	3.8	4.0	5.	4.5	5.3	4.8
Lu	0.51	0.43	0.57	0.45	0.63	0.55	0.69	0.72	0.73	0.77
Sc	32.	33.2	32.5	33.1	34.2	35.	28.5	27.7	28.1	28.2
Co	50.	49.3	47.9	44.5	47.3	43.	30.2	29.5	34.5	33.
Cr	130.	60.	34.2	29.	32.6	28.	9.2	88.	8.6	15.
Ni	70.	93.	43.4	43.	27.6	–	11.9	36.0	14.2	13.
Ta	1.05	1.05	1.33	1.35	1.51	1.56	1.37	1.73	1.55	2.13
Zr	189.	157.	202.	222.	226.	249.	279.	323.	292.	344.
Hf	4.4	3.8	4.9	5.3	5.5	6.	6.7	8.4	7.1	8.1
Th	1.22	1.15	1.55	1.53	1.74	2.03	2.81	3.59	2.83	3.0
Rb	10.0	6.	8.	11.	8.7	12.	16.	18.	16.3	21.
Sr	238.	320.	283.	308.	240.	288.	252.	261.	236.	296.

Fractionation step	Calc. 8B/6J	Obs. 6J	Calc. 8B/8V	Obs. 8V	Calc. 8V/8P	Obs. 8P	Calc. 8P/1A	Obs. 1A	Calc. 8P/18C	Obs. 18C
Res. Liq.	0.602		0.506		0.571		0.637		0.541	
Ol	0.033		0.035		0.044		0.012		0.022	
Pl	0.155		0.218		0.175		0.240		0.325	
Cpx	0.128		0.167		0.132		0.093		0.087	
Mt	0.077		0.072		0.065		0.013		0.019	
Ap	0.005		0.002		0.013		0.005		0.006	
Temp.	1,100.0		1,080.0		1,050.0		1,025.0		1025.0	
Log f_{O_2}	−9.5		−10.0		−10.5		−11.0		−11.0	
La	26.98	27.1	32.	34.	46.	41.	54.	70.	59.	70.
Ce	62.1	63.	76.9	84.	102.	100.	131.	146.	146.	153.
Sm	10.9	10.6	14.	12.8	12.8	11.7	14.5	21.5	15.9	22.
Eu	3.38	2.75	3.98	3.65	3.84	2.88	3.25	4.41	3.4	3.81
Tb	1.94	1.82	2.47	2.23	2.35	2.06	2.62	3.92	2.92	3.94
Yb	5.8	5.3	7.06	6.2	8.21	6.4	8.88	13.0	10.2	12.9
Lu	0.81	0.80	0.98	0.83	1.14	1.00	1.41	1.79	1.62	1.81
Sc	26.4	26.	24.7	25.1	19.7	12.1	12.2	4.5	13.9	2.0
Co	28.6	32.	29.5	30.3	18.4	8.2	9.2	–	9.0	0.58
Cr	5.4	71.	3.3	7.3	1.43	–	1.13	4.4	1.25	–
Ni	7.7	42.	5.6	–	0.09	–	1.2	0.73	0.67	–
Ta	1.46	1.99	1.67	2.67	2.79	2.75	3.75	6.1	4.2	5.6
Zr	312.	396.	358.	453.	611.	617.	882.	1,032.	1,017.	876.
Hf	7.5	9.	8.6	10.7	14.4	14.7	21.	25.7	24.2	23.5
Th	3.35	3.36	3.98	4.09	7.11	7.10	11.1	9.3	13.03	10.6
Rb	19.	23.	22.	26.	43.4	43.	63.5	54.	73.	67.
Sr	186.	270.	118.	282.	114.	194.	41.	91.	21.	64.

tribution coefficient data obtained from other rocks crystallizing under different conditions. Ideally, distribution coefficients would be obtained for minerals found in the rock suite studied, but such data are at present not available for Pinzon lavas. Selected distribution coefficients from the literature were used in the calculations (Table 5, Leeman 1974).

Given the trace element content of the assumed parent, reasonable estimates of the trace element content of each mineral phase, and calculated weight percent of each phase subtracted at each step of the differentiation series, one may calculate trace element contents for each of the derivative rocks. Such calculations were made using a simple computer program which included corrections for the effect of variations in temperature and oxygen fugacity on distribution coefficients for certain elements. The temperatures involved in various fractionation steps were estimated and the oxygen fugacities were assumed to correspond roughly to the QMF buffer at a given temperature (see Table 6). Because fractional crystallization is not likely to be represented by bulk equilibrium, but rather by surface equilibrium between crystal and liquid, the Rayleigh fractionation law (Gast 1968) was assumed to be applicable for calculating trace element abundances.

Table 6 shows a comparison between calculated and experimentally measured trace element abundances for different fractionation steps. In most cases, agreement between observed and calculated values is excellent. Possible sources of discrepancy include sampling problems, experimental error, and the possibility that many of the porphyritic rocks may not represent true liquids. However, it is likely that the largest errors in the calculated abundances are due to the uncertainty in mineral/liquid distribution coefficients.

The largest discrepancies occur for Sc and Sr. A distribution coefficient of 3.5 was used for $D_{Sc}^{cpx/liq.}$ in evaluating the mixes. This value proved approximately right for the less differentiated rocks, but somewhat low for the more evolved lavas. The distribution coefficient of Sc in clinopyroxene probably increases with decrease in temperature and/or differentiation as reported by Ewart et al. (1973) for clinopyroxenes from the Tongan Islands. An increase for the more evolved rocks would alleviate the disagreement between observed and calculated values for Sc.

The variation of $D_{Sr}^{plag/liq.}$ with temperature has been extensively studied by Drake (1972) and adjustments in accord with his experimental results have been used in the trace element computer tests. In general, the calculated abundances of Sr are too low when compared with observed abundances. More recent work indicates a compositional dependence of D_{Sr}^{plag}, which may in part explain the wide ranges of distribution coefficients for Sr which occur in the literature (McKay 1977). A reduction of 25% in the distribution coefficients determined by Drake for Sr in plagioclase results in much better fits and is also reasonable in light of some distribution coefficients reported in the literature (e.g., see Philpotts and Schnetzler 1970).

As pointed out earlier, some of the differentiated lavas of Unit N are anomalously rich in Cr and Ni (Fig. 9). This difference is also apparent in the mixes of a ferrobasalt of Unit R (DH-8B) to derive two lavas of Unit N (DH-17 and DH-6J) which were also tested by the trace element modeling. Reasonable fits occur for all elements except Ni and Cr, whose observed abundances are higher than those determined for the less evolved ferrobasalts. The melts which produced these icelandites may have been anomalously rich in these elements or the rocks were subject to a different crystallization history than were other lavas on the island. The most mafic lava found on Pinzon (PS-16) is distinguished by its unusually low excluded element contents and high Ni, Cr, and MgO contents. It is a possible parent for DH-8K, as indicated by relatively good major and trace element fits.

Thus, most of the lavas found on Pinzon appear to have compositions consistent with derivation by shallow-level fractional crystallization from a similar parental magma. The variations that do occur may be due to slightly varying conditions of crystallization (temperature, pressure, and oxygen fugacity) which might be expected during the volcano's history.

Acknowledgments. This work was supported largely by National Science Foundation Grant GZ-1895 and by several Geological Society of America Penrose Grants. I am indebted to G.G. Goles, A.R. McBirney, B.H. Baker, and F.J. Swanson for helpful discussions. A special note of thanks is due to Peter Kramer and the staff at the Charles Darwin Research Station for their assistance in the field.

References

Bryan, W.B., Finger, L.W., Chayes, F.: Estimating proportions in petrographic mixing equations by least-squares approximation. Science **163**, 926–927 (1969)

Carmichael, I.S.E.: The petrology of Thingmuli, a Tertiary volcano in Eastern Iceland. J. Petrol. **5**, 435–460 (1964)

Chayes, F.: A petrographic distinction between Cenezoic volcanics in and around the open oceans. J. Geophys. Res. **69**, 1573–1588 (1964)

Chubb, L.J.: Geology of the Galapagos, Cocos, and Easter Islands. B.P. Bishop Mus. Bull. **180**, 67 pp. (1930)

Drake, M.J.: The distribution of major and trace elements between plagioclase feldspar and magmatic silicate liquid: an experimental study. Ph. D. dissertation, University of Oregon, 190 pp. (1972)

Ewart, A., Bryan, W.B., Gill, J.B.: Mineralogy and geochemistry of the younger volcanic islands of Tonga, S.W. Pacific. J. Petrol. **14**, 429–465 (1973)

Gast, P.W.: Trace element fractionation and the origin of tholeiitic and alkaline magma types. Geochim. Cosmochim. Acta **32**, 1057–1086 (1968)

Gordon, G.E., Randle, K., Goles, G.G., Corliss, J.B., Beeson, M.H., Oxley, S.S.: Instrumental activation analysis of standard rocks with high resolution X-ray detectors. Geochim. Cosmochim. Acta **32**, 369–396 (1968)

Haskin, L.A., Haskin, M.A., Frey, F.A., Wildeman, T.R.: Relative and absolute terrestrial abundances of the rare earths. In: Origin and Distribution of the Elements (L.H. Ahrends, ed.), pp. 889–912. Pergamon 1968

Irvine, T.N., Baragar, W.R.A.: A guide to the chemical classification of the common volcanic rocks. Can. J. Earth Sci. **8**, 523–548 (1971)

Komar, P.D.: Mechanical interactions of phenocrysts and flow differentiation of igneous dikes and sills. Bull. Geol. Soc. Am. **83**, 973–988 (1972)

Leeman, W.P.: Petrology of basalts from the Snake River Plain, Idaho, and experimental determination of partitioning of divalent cations between olivine and basaltic liquid. Ph. D. dissertation, University of Oregon, 337 pp. (1974)

Lindstrom, M.M.: Geochemical studies of volcanic rocks from Pinzon and Santiago Islands, Galapagos Archipelago. Ph. D. dissertation, University of Oregon, 174 pp. (1976)

Macdonald, G.A., Katsura, T.: Chemical composition of Hawaiian lavas. J. Petrol. **5**, 82–133 (1964)

McBirney, A.R., Williams, H.W.: Geology and petrology of the Galapagos Islands. Geol. Soc. Am., Mem. **118**, 197 pp. (1969)

McKay, G.: The petrogenesis of titanium-rich basalts from the lunar maria and of KREEP-rich rocks from the lunar highlands. Ph. D. dissertation, University of Oregon, 230 pp. (1977)

Moore, J.G.: Development of pillows on the submarine extension of recent lava flows, Mount Etna, Sicily. U.S. Geol. Surv., Prof. Pap. **750**-C, c89–c97 (1971)

Norrish, K., Hutton, J.T.: An accurate X-ray spectrographic method for the analysis of a wide range of geological samples. Geochim. Cosmochim. Acta **33**, 431–453 (1969)

Philpotts, J.A., Schnetzler, C.C.: Phenocryst-matrix partition coefficients for K, Rb, Sr, and Ba, with applications to anorthosite and basalt genesis. Geochim. Cosmochim. Acta **34**, 307–332 (1970)

Rucklidge, J.: A computer program for processing microprobe data. J. Geol. **75**, 126 (1967)

Schilling, J.G.: Sea-floor evolution: rare-earth evidence. Phil. Trans. R. Soc. Lond. A. **268**, 663–706 (1971)

Simkin, T.: Flow differentiation in the picrite sills of North Skye. In: Ultramafic and Related Rocks (P.J. Wylie, ed.), pp. 64–69. New York: Wiley 1967

Swanson, F.J., Baitis, H.W., Lexa, J., Dymond, J.: Geology of Santiago, Rabida, and Pinzon Islands, Galapagos. Bull. Geol. Soc. Am. **85**, 1803–1810 (1974)

Thornton, C.P., Tuttle, O.F.: Chemistry of igneous rocks: pt. I, differentiation index. Am. J. Sci. **258**, 664–685 (1960)

Yoder, H.S., Tilley, C.E.: Origin of basalt magmas: an experimental study of natural and synthetic rock systems. J. Petrol. **3**, 343–532 (1962)

Received February 1, 1979; Accepted January 18, 1980